Received: 5 August 2020 | Revised: 5 August 2020 | Accepted: 18 August 2020

DOI: 10.1111/ijac.13625

ORIGINAL ARTICLE

International Journal of Applied Ceramic TECHNOLOGY

Extraction and characterization of hydroxyapatite-based materials from grey triggerfish skin and black scabbardfish bones

Pedro Ideia[1] | **Lorenzo Degli Esposti**[2] | **Carla Caseiro Miguel**[1] | **Alessio Adamiano**[2] | **Michele Iafisco**[2] | **Paula C. Castilho**[1]

[1]CQM – Centro de Química da Madeira, Universidade da Madeira, Funchal, Portugal

[2]ISTEC – Institute of Science and Technology for Ceramics, National Research Council (CNR), Faenza, Italy

Correspondence
Paula C. Castilho, CQM – Centro de Química da Madeira, Universidade da Madeira, Campus da Penteada, 9020-105 Funchal, Portugal.
Email: pcastilho@staff.uma.pt

Abstract

The conversion of food industry by-products to compounds with high added value is nowadays a significant topic, for social, environmental, and economic reasons. In this paper, calcium phosphate-based materials were obtained from black scabbardfish (*Aphanopus carbo*) bones and grey triggerfish (*Balistes capriscus*) skin, which are two of the most abundant fish by-products of Madeira Island. Different calcination temperatures between 400 and 1000°C were employed. Materials obtained from calcination of bones of black scabbard fish were composed by homogeneous mixtures of hydroxyapatite ($Ca_{10}(PO4)_6(OH)_2$, HAp) and β-tricalcium phosphate (β-$Ca_3(PO_4)_2$, β-TCP). Because of the high biocompatibility of HAp and the good resorbability of β-TCP, these natural biphasic materials could be very relevant in the field of biomaterials, as bone grafts. The ratio between HAp and β-TCP in the biphasic compound was dependent on the calcination temperature. Differently, the material obtained from skin of grey triggerfish contained HAp as the main phase, together with small amounts of other mineral phases, such as halite and rhenanite, which are known to enhance osteogenesis when used as bone substitutes. In both cases, the increase of calcination temperature led to an increase in the particles size with a consequent decrease in their specific surface area. These results demonstrate that from the fish by-products of the most consumed fishes in Madeira Island it is possible to obtain bioceramic materials with tunable composition and particle morphology, which could be promising materials for the biomedical field.

KEYWORDS

biomaterials, bones, calcium phosphate, fish by-products, hydroxyapatite, scales

1 | INTRODUCTION

Fish processing industry (FPI) produces large amounts of by-products every year, which can account for up to 75 wt% of the catch depending on postharvest or industrial preparation processes.[1] The conversion of fish by-products such as heads, bones, skins, and viscera, into economically attractive products could contribute to a more sustainable FPI.[1-4]

In this domain, some of the most abundant by-products such as fish scales and bones, have an high content of mineral phase, mainly in the form of hydroxyapatite [$Ca_{10}(PO_4)_6(OH)_2$ – HAp].[5] Due to its excellent biocompatibility with human tissue, HAp can be used to prepare calcium phosphate-based bioceramics which have been

Pedro Ideia and Lorenzo Degli Esposti contributed equally.

extensively used in the biomedical field in the last 20 years as coating of metallic prostheses, as cement for bone and dental implant, and as massive three-dimensional bone substitutes.[6-10] Biphasic mixtures of HAp and other calcium phosphate crystal phases, such as tricalcium phosphate [$Ca_3(PO_4)_2$ – TCP], have been widely used as bone grafts in virtue of their superior behavior in comparison to HAp alone in terms of tunable resorption, bioactivity, and intrinsic osteoinduction.[6,11-13] Several methodologies for the preparation of synthetic HAp and TCP as well as their mixtures are reported in the literature.[14-16] Most of the procedures to obtain HAp/TCP biphasic mixtures are based on the chemical reaction between calcium and phosphorous sources, followed by a thermal treatment of the synthesis product.[6]

The extraction of HAp/TCP biphasic mixtures from by-products of fishery industry (ie, fish bone) has been also recently investigated as a safer, cheaper, and simpler procedure. It was demonstrated that calcium phosphates obtained from natural sources, having a nonstoichiometric composition and a disordered nanostructure[17] are more biocompatible[2] and display a better metabolic activity with respect to stoichiometric ones.[18,19] Furthermore, another advantage of biogenic calcium phosphates is that they may contain microelements such as magnesium or strontium, that were proved to have a stimulatory effect on bone formation both in vitro and in vivo.[20,21] The most common method for extracting calcium phosphate-based materials from fish by-products is the thermal calcination,[6,12,22-25] even if other methods such as alkaline[22,26] and enzymatic hydrolysis[27] can be used as well.

In the present study, solid-state mixtures of HAp and other calcium phosphate phases (ie, TCP and rhenanite [$NaCaPO_4$ – Rhe]) were obtained by thermal calcination of grey triggerfish (*Balistes Capriscus)* skin and black scabbardfish *(Aphanopus Carbo)* bones at various temperatures. Both these species are among the most consumed fishes in Madeira Island, where the high quantities of their respective by-products have a significant impact on the local environment and economy. As an example, in January 2017, black scabbardfish constituted the 85.7% of the total fishing at Madeira Island for an amount of 245 tons.[28] Although grey triggerfish capture is less intensive, it still is relevant in terms of by-products production. Morphological parts were selected based on the abundance of residues, while scabbardfish is sold as boneless fillets fresh or frozen, its thin fatty skin discarded, and grey triggerfish is sold whole with its thick harsh skin removed. In this paper, calcium phosphate bioceramics obtained from *B capriscus* skin and *A carbo* bones materials were characterized to evaluate the effect of calcination temperature on their chemical and crystallographic composition, particle size, and surface area. It was revealed that both materials have interesting properties for producing bioceramic materials for biomedical application due to the presence of osteoinductive components such as β-TCP, rhenanite, Mg^{2+}, and Sr^{2+} ions. Furthermore, it was established that calcination temperature allows to control the properties of these materials. These data are very relevant, since in the future it is intended to use these materials as scaffolds for osteogenic differentiation of mesenchymal stem cells.

2 | MATERIALS AND METHODS

2.1 | Biological material

Black scabbardfish (SF) by-products were collected from a local market in Funchal (Madeira Island, Portugal). The bones were separated and washed under running water and manually scraped to remove adhering tissues. After grinding in a hand miller, bones were stored at −20°C for further use.

Grey triggerfish (TF) skin samples were obtained from specimen captured along the coast of Funchal. Immediately after capture, the skin was collected and stored in polyethylene bags at −20°C. Before being used for experiments, skin samples were washed under tap water and cut into small pieces. Commercial hydroxyapatite (for analysis, >95% pure, CAS Number 1306-06-5, MW 502.31 g mol^{-1}) was purchased by ACROS Organics (Geel, Belgium).

2.2 | Isolation of HAp by thermal calcination

Bones and skin samples were thermally treated at 400, 600, 800, and 1000°C to evaluate the impact of temperature on the extraction yield and on the properties of the obtained materials. Heating was performed in air using a Nabertherm furnace (Germany), with a heating ramp of 15°C min^{-1} and with an annealing time of 4 hours. All the thermal treatments were performed in duplicates.

2.3 | Characterization of isolated HAp

Crystalline phases of the different samples were identified and quantified by Powder X-Ray Diffraction (PXRD; D8 Advance diffractometer, Bruker, Karlsruhe, Germany) equipped with a Lynx-eye position sensitive detector. PXRD pattern were recorded using Cu$K\alpha$ radiation ($\lambda = 1.54178$ Å) generated at 40 kV and 40 mA, collecting in the 2θ range from 10° to 80° with a step size (2θ) of 0.02 and a counting time of 1 second. Quantitative evaluation of phase compositions was performed by full-profile Rietveld analysis of the PXRD diffractograms (TOPAS v. 5.0, Bruker AXS, Karlsruhe, Germany).[29] Each crystalline phase composition

was refined using tabulated atomic coordinates,[30-33] and symmetrized spherical harmonics were used to cope, phenomenologically, with HAp anisotropic peak broadening effects due to the anisotropic crystal shape. The PXRD patterns background were calculated as 11th order Chebychev function.

Fourier transform infrared spectra of the powders were collected in attenuated total reflectance mode (Perkin Elmer Spectrum Two FT-IR spectrometer coupled with a Zn/Se UATR accessory; PerkinElmer; Massachusetts, USA), over the range 400-4000 cm^{-1} with a resolution of 4 cm^{-1} by accumulation of 16 scans.

The amount of organic matter in the samples was determined as difference between the weight of the treated materials and the weight of the samples after thermal treatment at 1100°C for 2 hours.

Quantification of Ca, P, Mg, Sr, and Na was carried out by inductively coupled plasma optical emission spectrometry (ICP-OES) (Agilent Technologies 5100 ICP-OES, Santa Clara, CA, USA). Samples were prepared by dissolving an aliquot of powder in a 1 wt% HNO_3 solution. Atomic emission was measured at the following wavelengths: Ca 422.673 nm, P 213.618 nm, Mg 279.553 nm, Sr 407.771 nm, Na 588.995 nm.

The three-dimensional topography analysis of the materials obtained after calcination of TF skin at 800°C was evaluated by scanning electron microscopy (SEM) (Phenom ProX Desktop SEM, Thermo Fisher Scientific, Waltham, MA, USA). The samples were deposited on copper tape, mounted on an aluminum SEM stub. Accelerating voltages between 5 and 15 kV was used to observe the samples in secondary electron imaging mode. Randomly selected regions were recorded for each sample.

The morphology of the nano- and microcrystals deriving from the thermal treatment of bones and skin was evaluated by scanning electron microscopy with a field-emission microscope (FEG-SEM, mod. ΣIGMA, ZEISS NTS Gmbh, Oberkochen, Germany). The powdered samples were deposited on a carbon tape mounted on an aluminum SEM stub and sputter-coated (Polaron E5100, Polaron Equipment, Watford, Hertfordshire, UK) with 10 nm of gold in order to provide electrical conductance. Accelerating voltages of 3 kV was used to observe the samples in secondary electron imaging mode. Randomly selected regions (minimum four) at magnifications of 10 000×, 25 000×, and 50 000× were recorded for each sample.

Specific surface area (SSA) of the powdered samples was measured through N_2 gas adsorption modeled by the Brunauer–Emmett-Teller (BET) method.[34] BET N_2 gas adsorption method was employed using a Surfer instrument (Thermo Fisher Scientific Inc, Waltham, MA, USA). Before measurement, samples were degassed at 100°C for 3 hours under vacuum.

3 | RESULTS AND DISCUSSION

3.1 | Characterization of isolated HAp

HAp-based materials were obtained by thermal calcination, heating the fish by-products for 4 hours at four different temperatures, namely 400, 600, 800 and 1000°C, with a heating slope of 15°C/min.

PXRD pattern of the samples isolated from TF skin at different temperatures are shown in Figure 1A. The pattern of the material obtained at 400°C is characterized by very broad and poorly defined diffraction peaks, that were indexed as diffraction peaks of HAp (PDF card file 00-009-0432), together with low-intensity peaks of halite (Hal, NaCl, PDF card file 00-005-0628). Multiphase Rietveld refinement revealed that the sample of TF skin treated at 400°C was composed by ca. 95 wt% of poorly crystalline HAp and ca. 5 wt% of Hal. Also the samples obtained at 600 and 800°C are characterized by HAp as the main crystalline phase and Hal as the secondary phase, together with traces of rhenanite (Rhe, $NaCaPO_4$, PDF card file 00-029-1193) and β-TCP (PDF card file 00-009-0169), where the latter is present only in the sample treated at 600°C. The sample calcined at 1000°C consisted almost entirely of HAp, with small amounts of magnesium oxide (MgO) and cubic trisodium phosphate (γ-Na_3PO_4) (accounting together for less than 5 wt%). In a previous work, Piccirillo et al also studied the calcination of fish scales of sardine (*Sardina pilchardus*), reporting the presence of halite, whose amount decreased with the increase of calcination temperature.[24] A similar trend was reported for materials isolated from codfish (*Gadus morhua*) bones[35] and, more recently, from hairtail (*Trichiurus lepturus*) bones.[36] With the increase of calcination temperature, the HAp contained in the samples derived from TF skin displays more intense and sharper peaks. This reveals an increase of structural order and crystal growth upon increase of calcination temperature. In terms of crystallinity, TF skin samples treated at 600°C, 800°C and 1000°C are very similar to a commercial hydroxyapatite material, presenting narrow and well-defined peaks.

With the exception of the sample obtained at 400°C, the PXRD patterns of the samples derived from SF bones (Figure 1B) featured the presence of only HAp and β-TCP peaks. The β-TCP content increases with the increase of calcination temperature, ranging from 17.5 wt% at 600°C to 29.7 wt% at 800°C, and to 40.1 wt% at 1000°C. Also in this case, the samples of SF bones treated at 600°C, 800°C, and 1000°C contained HAp with narrow and well-defined peaks, very similar to the commercial hydroxyapatite.

Piccirillo et al[24] observed a similar trend with calcination temperature on sardine bones by-products. The formation of biphasic materials of HAp/β-TCP through calcination and sintering of fish bones by-products is widely

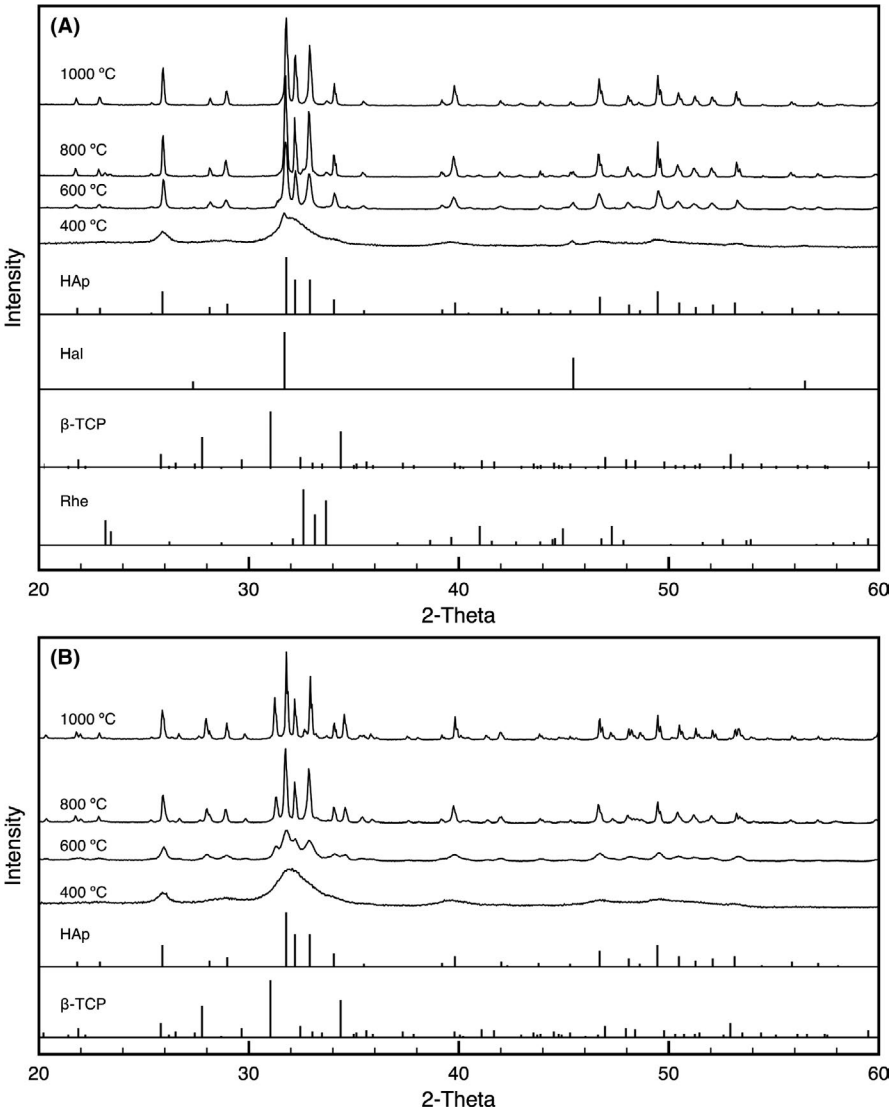

FIGURE 1 PXRD pattern of the samples obtained by calcination of (A) TF skin and (B) SF bones, together with the reference patterns of HAp (00-009-0432), β-TCP (00-009-0169), Hal (00-005-0628), and Rhe (00-029-1193)

reported in the literature.[6,12,35] This is due to the nonstoichiometric nature of biogenic HAp, where the calcium deficiency induces the formation of β-TCP phase that has a lower Ca/P ratio. Also Rhe can be formed by recrystallization of HAp grains (Ca-deficient, Na-riched).[37] Rhe has been suggested to be a better osteogenesis enhancer than β-TCP.[38] In fact, because of their high biocompatibily and bioactivity, Rhe formulations have already been commercialized for orthopedic surgery proposes.[39] In this respect, the presence of β-TCP and Rhe in these samples due to the nonstoichiometric composition of the starting material might be an advantage, since both secondary phases could enhance the biological response of the bioceramic product in comparison to a pure HAp product.

FT-IR spectra of commercial HAp and the samples obtained by calcination of TF skin and SF bones are reported in Figure 2.

Bands at 471 cm^{-1}, 562 cm^{-1}, and 600 cm^{-1} were associated to double and triple degenerated bending modes of the O-P-O bonds of the phosphate group. The peak at around 626 cm^{-1} was due to vibrational mode of hydroxyl groups of Hap.[40] The weak band around 961 cm^{-1} was related to non-degenerated symmetric stretching mode of the P-O bond of the phosphate groups. The broad band in region 1025-1032 cm^{-1} was associated to the triply degenerated asymmetric stretching mode of the P-O bond of PO_4 groups. The peaks in the region 1093-1047 cm^{-1} were due to PO_4^{3-} stretching mode.[12,26,27,40].Bending and stretching mode of carbonate ions were witnessed by the presence of small peaks at 870-880 cm^{-1} and 1400-1500 cm^{-1},[40] typical of biogenic HAp, that is naturally enriched with carbonate ions.[12]

Peaks at 947, 978 and 1119 cm^{-1} were detected in the samples of TF skin treated at 600°C and in those of SF bones treated at 600°C, 800°C, and 1000°C. These three peaks, marked by black arrows in Figure 2, are not present in commercial HAp spectra and are characteristic of β-TCP[40,41] in agreement with PXRD results.

After normalization of the spectra of SF derived samples on the main phosphate band (~1025 cm^{-1}), it is clear that the intensity of peaks at 947, 978, and 1119 cm^{-1} increased

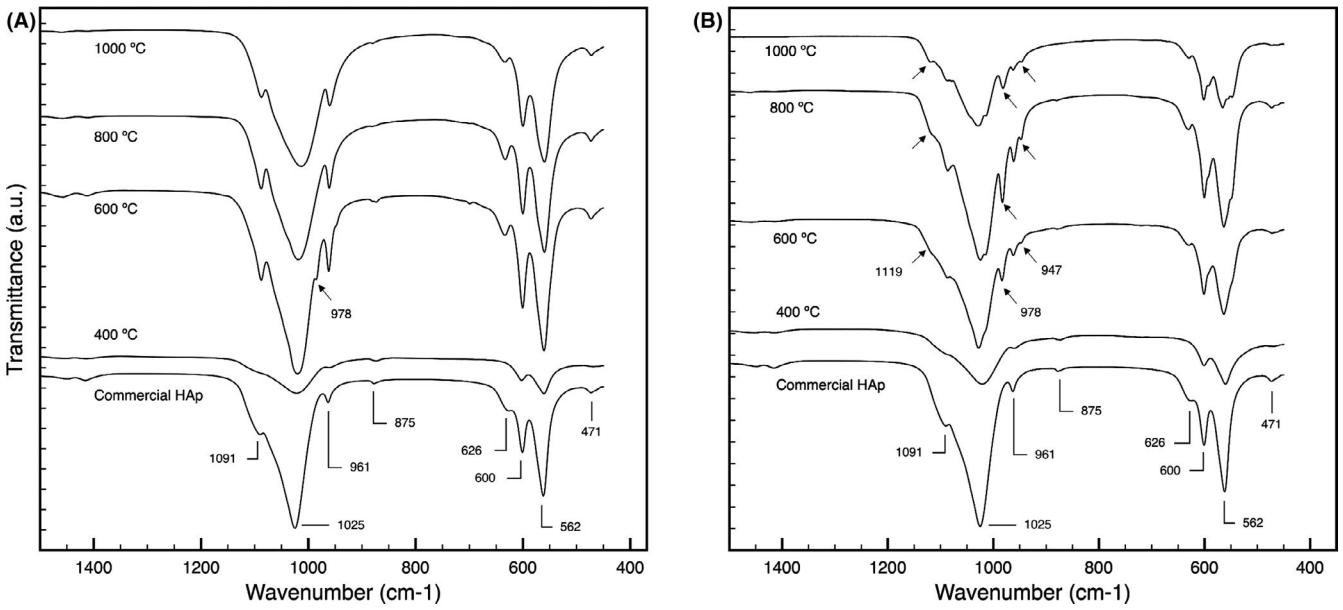

FIGURE 2 Fourier transform infrared spectra for commercial hydroxyapatite and the samples obtained by calcination of (A) TF skins, and (B) SF bones. Black arrows indicate the peaks of β-TCP

with the increase of calcination temperature (Figure S1). This trend confirms the increase of β-TCP phase content with calcination temperature observed by PXRD (Table 1).

Table 2 shows the chemical composition of the calcined samples. The extraction yield (% w/w) of the materials obtained from TF skin decreased with the increasing calcination temperature from 26.3 to 17.6 wt% (dry weight) for 400 and 1000°C, respectively. The same trend was observed for materials obtained from the thermal treatment of SF bones, for which the extraction yields were 49.1% for calcination at 400°C and 34.3% for calcination at 1000°C. The apparent decrease of extraction yield is due to the presence of organic matter residuals in 400°C samples (ca. 20-40 wt%), that increase the weight of the final product. In all the samples, the most abundant elements were Ca and P, with a minor amount of Na, and traces of Mg and Sr The relative abundance of these elements increases with the increase of calcination temperature proportionally to the decrease of the organic matter.

Samples obtained from the calcination of TF skin have a Ca/P molar ratio slightly lower than stoichiometric HAp (1.67). Biogenic HAp are commonly Ca -deficient, where foreign ions such as Mg^{2+} and Sr^{2+} partially replace Ca^{2+} in the HAp structure.[42] This also occurs in the case of TF skin samples, since the (Ca + Mg + Sr)/P ratio was found to be very close to 1.67, indicating that Mg^{2+} and Sr^{2+} are present in the HAp structure of TF skin.

SF bone-derived samples have a (Ca + Mg + Sr)/P molar ratios significantly lower than 1.67, indicating that these materials have a different chemical composition with respect to those extracted from TF skin. Furthermore, the low (Ca + Mg + Sr)/P molar ratio of SF bones samples is in agreement with the formation with calcination of HAp/β-TCP mixtures as described above.

Figure 3A shows the macroscopic appearance of the solids obtained after calcination of TF skin at 800°C. Interestingly, even after thermal treatment the sample

TABLE 1 Quantification of crystalline phases (reported as wt. %) of samples obtained by calcination of TF skin and SF bones by multiphase Rietveld refinement

Calcination temperature	400°C	600°C	800°C	1000°C
TF skin				
Hap	95.5 ± 0.2	86.2 ± 0.4	89.4 ± 0.3	95.8 ± 0.3
Hal	4.5 ± 0.2	4.1 ± 0.1	2.2 ± 0.1	—
β-TCP	—	4.6 ± 0.2	—	—
Rhe	—	5.0 ± 0.3	8.4 ± 0.3	—
Other phases	—	—	—	4.2 ± 0.3
SF bones				
Hap	100.0 ± 0.0	82.5 ± 0.3	70.3 ± 0.3	59.9 ± 0.2
β-TCP	—	17.5 ± 0.3	29.7 ± 0.3	40.1 ± 0.2

Abbreviations: Hal, halite; Hap, hydroxyapatite; Rhe, rhenaniteβ-TCP, β-tricalcium phosphate.

TABLE 2 ICP-OES data, organic matter content and extraction yield for samples obtained by calcination of TF skin and SF bones

Calcination temperature	400°C	600°C	800°C	1000°C
TF skin				
Ca wt%	26.20 ± 0.70	37.20 ± 0.05	38.60 ± 0.40	38.70 ± 0.20
P wt%	12.30 ± 0.20	17.80 ± 0.20	18.30 ± 0.20	18.40 ± 0.20
Mg wt%	0.58 ± 0.05	0.73 ± 0.01	0.66 ± 0.01	0.76 ± 0.01
Sr wt%	0.13 ± 0.01	0.17 ± 0.01	0.17 ± 0.01	0.18 ± 0.01
Na wt%	2.19 ± 0.07	2.92 ± 0.06	2.24 ± 0.04	1.17 ± 0.01
Ca/P ratio	1.65 ± 0.03	1.62 ± 0.01	1.63 ± 0.01	1.62 ± 0.01
(Ca + Mg+Sr)/P ratio	1.72 ± 0.04	1.67 ± 0.01	1.68 ± 0.01	1.68 ± 0.01
Organic matter wt%	35.60 ± 0.50	6.66 ± 0.09	3.40 ± 0.05	0.15 ± 0.01
SF bones				
Ca wt%	29.00 ± 0.80	37.80 ± 0.40	38.60 ± 0.40	38.70 ± 0.50
P wt%	15.30 ± 0.50	19.00 ± 0.20	19.40 ± 0.30	19.40 ± 0.20
Mg wt%	0.60 ± 0.02	0.76 ± 0.01	0.77 ± 0.01	0.78 ± 0.01
Sr wt%	0.14 ± 0.01	0.18 ± 0.01	0.18 ± 0.01	0.18 ± 0.01
Na wt%	1.14 ± 0.11	0.93 ± 0.01	0.99 ± 0.02	0.95 ± 0.00
Ca/P ratio	1.47 ± 0.01	1.54 ± 0.01	1.54 ± 0.01	1.54 ± 0.01
(Ca + Mg+Sr)/P ratio	1.52 ± 0.01	1.59 ± 0.01	1.59 ± 0.01	1.59 ± 0.01
Organic matter wt%	20.00 ± 0.20	3.86 ± 0.04	1.55 ± 0.02	0.78 ± 0.01

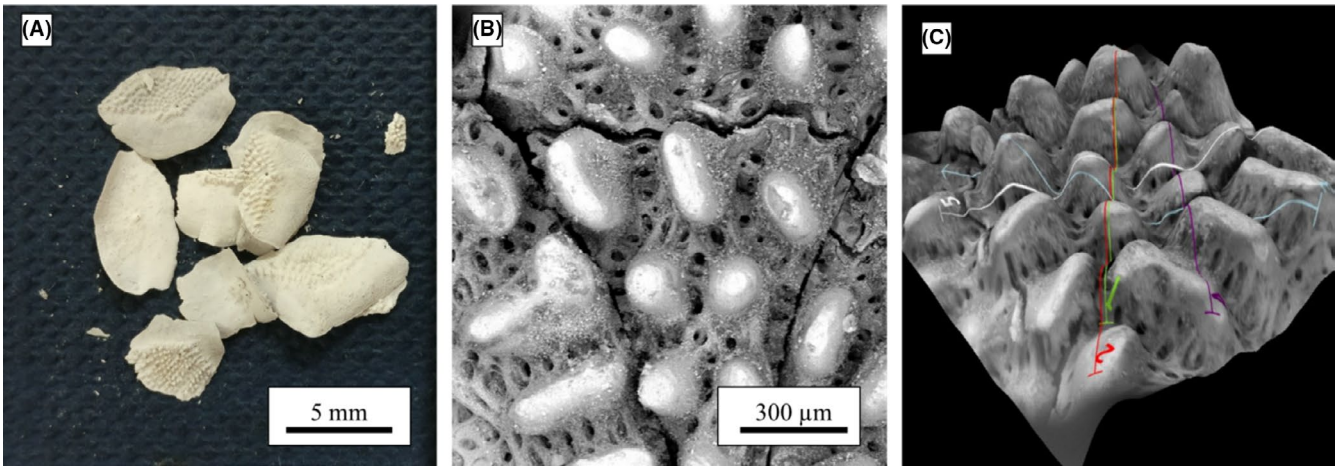

FIGURE 3 A, Macroscopic appearance of the materials obtained by calcination of triggerfish skin at 800°C. B, SEM micrographs of the hydroxyapatite at magnification of 200×. C, 3D topographic analysis of the sample [Color figure can be viewed at wileyonlinelibrary.com]

presented the same structure of the pristine material, and was composed of individual scales with ca. 1 cm in length and ca. 0.4 cm in width. The inner face of the scales was completely smooth while the outer face had a rough region, with protuberances that give the skin a sandpaper-like texture, as observed by SEM microscopy and three-dimensional topography analysis (Figure 3B,C). SEM three-dimensional topography analysis of the micrographs revealed that the protuberances were 100-360 µm high and were separated by a microporous structure (around 35 µm in diameter) between them. To the best of our knowledge, it is the first time this unique microstructure is observed. Due to the thin microstructure of calcined scales, the materials could be easily reduced to powders.

Particle morphology of TF skin and SF bone-derived samples was analyzed by FEG-SEM microscopy (Figure 4). Micrographs were collected only on the powders treated at temperature above 600°C, because the samples treated at 400°C were too rich of organic matter to clearly show the morphology of inorganic particles (see Figure S2). Micrographs showed that for both the by-products, the increase of calcination temperature resulted in an increase of particles size as a consequence of growth of grains. In terms of size, the particles obtained from the calcination of SF bones were always

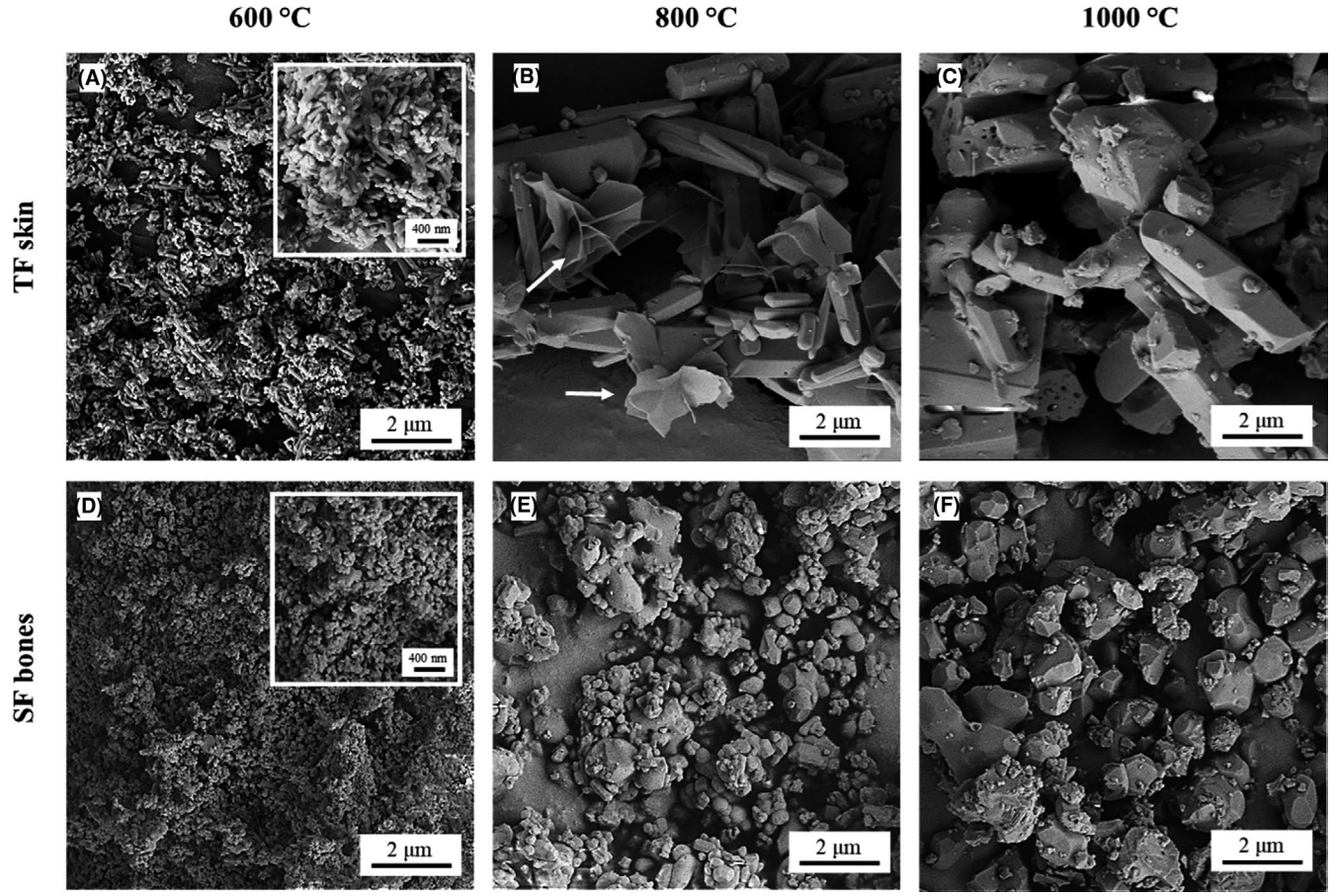

FIGURE 4 SEM micrographs (25 000× magnification) of powders obtained from TF skin and SF bones by calcination at 600, 800, and 1000°C. Insets: high magnification (100 000× magnification) of samples calcined at 600°C with evidence for (A) rod-like and (D) isotropic morphology. Arrows indicate the flower-like Rhe crystals.

smaller than those obtained from TF skin independently of calcination temperature.

The micrograph of the samples of TF skin treated at 600°C (Figure 4A and inset) shows that the sample is constituted of elongated, rod-like submicrometric HAp crystals, ca. 200-400 nm in length and ca. 100 nm in width. With the increase of calcination temperature, the crystals considerably grow while preserving their rod-like morphology (Figure 4B,C). In the samples treated at 600 and 800°C it is evident that the crystalline rods have a hexagonal prism morphology, in agreement with HAp hexagonal crystal symmetry. Micrograph of the samples of TF skin treated at 800°C also shows the presence of a secondary flower-like morphology (see arrows in Figure 4B), that was attributed to Rhe crystals.

Micrograph of the samples of SF bones treated at 600°C (Figure 4D and inset), on the other hand, shows that the sample is constituted by crystals of less than 100 nm in diameter that are smaller and more isotropic than those of TF skin. Also the crystals from SF bones grow in size with the increase of calcination temperature, without changing their morphology (Figure 4D,E,F).

The increase of calcination temperature for both SF bones and TF skin samples resulted in a decrease of their specific surface area (SSA), as reported in Table 3 (nitrogen adsorption isotherms in Figure S3). The powder obtained from the calcination of TF skin at 400°C presented a SSA_{BET} of 110.42 $m^2 g^{-1}$, which decreased to 13.77, 2.45, and 2.10 $m^2 g^{-1}$ for powders obtained at 600°C, 800°C, and 1000°C, respectively. The same trend was observed for the samples of SF bones, for which the SSA_{BET} decreased from 133.47 $m^2 g^{-1}$ (400°C) to 2.53 $m^2 g^{-1}$ (1000°C). The decrease of the SSA_{BET} is related to increase in the particle size, as shown by FEG-SEM (Figure 4). A similar result was obtained by Jalota, Bhaduri and Tas [43] after calcination of biphasic materials

TABLE 3 Specific surface area (BET method) of samples obtained by calcination of TF skin and SF bones

	Specific surface area ($m^2 g^{-1}$)	
Calcination temperature	**TF skin**	**SF bones**
400°C	110.4 ± 11.0	133.5 ± 13.0
600°C	13.8 ± 1.4	31.0 ± 3.0
800°C	2.5 ± 0.2	4.8 ± 0.5
1000°C	2.1 ± 0.2	2.5 ± 0.3

at different temperatures. Bernache-Assolant et al[44] also established a relation between the calcination temperature and the decrease of SSA_{BET}. In both studies, authors reported a surface area of around 30-35 $m^2\ g^{-1}$ for powders calcined at 600°C. In the case of samples obtained at 400°C, the much larger SSA_{BET} is ascribable to the HAp nanocrystalline structure and the formation of a large amount of porous charcoal (also referred to as bone char) due to the incomplete combustion of the original organic matter in fish skin and bones.[45]

4 | CONCLUSIONS

Calcium phosphate-based materials were successfully obtained for the first time from the thermal treatment of grey triggerfish and black scabbardfish by-products. The isolated materials were found to possess different particles morphologies, chemical and crystallographic composition that varied with the nature of the by-products and calcination conditions. In particular, HAp-based materials were obtained from the thermal treatment of TF skin. In addition to HAp, Rhe was also detected in samples obtained from the thermal treatment of TF skin at 600°C and 800°C. Thermal treatment of SF bones, on the other hand, led to the production of biphasic (HAp/β-TCP) mixtures, where the temperature of calcination was proved to control the composition of the mixtures. The increase in calcination temperature led to an increase of particle size and a decrease in the specific surface area for the samples from both TF skin and SF bones. The presence of β-TCP and Rhe in HAp-based mixtures is particularly interesting for applications in the field of regenerative materials, because it may enhance osteogenesis process by affecting cell adhesion and proliferation. In this respect, the reported materials could find interesting applications for the production of 3D biomedical scaffolds and as bone fillers. Furthermore, as the reported biomaterials were produced from FPI residues, this work constitutes an interesting example of circular economy involving the development of high added value compounds with financial and environmental advantages for a more sustainable FPI.

ACKNOWLEDGMENTS

This work was supported by FCT-Fundação para a Ciência e a Tecnologia (projectPEst-OE/QUI/UI0674/2019, CQM, Portuguese Government funds), and through Madeira 14-20 Program, project PROEQUIPRAM—Reforço do Investimento em Equipamentos e Infraestruturas Científicas na RAM (M1420-01-0145-FEDER-000008) and by ARDITI-Agência Regional para o Desenvolvimento da Investigação Tecnologia e Inovação, through the project M1420-01-0145-FEDER-000005—Centro de Química da Madeira—CQM+ (Madeira 14-20). Pedro Ideia is the recipient of a PhD Grant under the project M1420-09-5369-FSE-000001.

ORCID

Pedro Ideia https://orcid.org/0000-0002-2178-2262
Lorenzo Degli Esposti https://orcid.org/0000-0002-6596-560X
Carla Caseiro Miguel https://orcid.org/0000-0002-1798-1154
Alessio Adamiano https://orcid.org/0000-0002-2077-0411
Michele Iafisco https://orcid.org/0000-0002-7813-8347
Paula C. Castilho https://orcid.org/0000-0002-8303-4286

REFERENCES

1. Rustad T, Storrø I, Slizyte R. Possibilities for the utilisation of marine by-products: Utilisation of marine by-products. Int J Food Sci Technol. 2011;46(10):2001–14.
2. Ideia P, Pinto J, Ferreira R, Figueiredo L, Spínola V, Castilho PC. Fish processing industry residues: a review of valuable products extraction and characterization methods. Waste and Biomass Valorization. 2020;11(7):3223–46; Disponível em: http://link.springer.com/10.1007/s12649-019-00739-1.
3. Adeoti IA, Hawboldt K. A review of lipid extraction from fish processing by-product for use as a biofuel. Biomass Bioenergy. 2014;63:330–40.
4. Olsen RL, Toppe J, Karunasagar I. Challenges and realistic opportunities in the use of by-products from processing of fish and shellfish. Trends Food Sci Technol. 2014;36(2):144–51.
5. Toppe J, Albrektsen S, Hope B, Aksnes A. Chemical composition, mineral content and amino acid and lipid profiles in bones from various fish species. Comp Biochem Physiol B Biochem Mol Biol. 2007;146(3):395–401.
6. Piccirillo C, Pullar RC, Costa E, Santos-Silva A, Pintado MME, Castro PML. Hydroxyapatite-based materials of marine origin: A bioactivity and sintering study. Mater Sci Eng C. 2015;51:309–15.
7. Tripathi G, Basu B. A porous hydroxyapatite scaffold for bone tissue engineering: physico-mechanical and biological evaluations. Ceram Int. 2012;38(1):341–9.
8. Li C, Born A-K, Schweizer T, Zenobi-Wong M, Cerruti M, Mezzenga R. Amyloid-hydroxyapatite bone biomimetic composites. Adv Mater. 2014;26(20):3207–12.
9. Iafisco M, Bosco R, Leeuwenburgh SCG, van den Beucken JJJP, Jansen JA, Prat M, et al. Electrostatic spray deposition of biomimetic nanocrystalline apatite coatings onto titanium. Adv Eng Mater. 2012;14(3):B13–20.
10. Baino F, Ferraris M. Learning from Nature: Using bioinspired approaches and natural materials to make porous bioceramics. Int J Appl Ceram Technol. 2017;14(4):507–20.
11. Garavelli CL, Melone N, Nuovo G. Presence of whitlockite in the mineral substance of annealed fish-bones: character and possible significance. Oceanol Acta. 1979;2(4):417–22.
12. Boutinguiza M, Pou J, Comesaña R, Lusquiños F, de Carlos A, León B. Biological hydroxyapatite obtained from fish bones. Mater Sci Eng C. 2012;32(3):478–86.
13. Terzioğlu P, Öğüt H, Kalemtaş A. Natural calcium phosphates from fish bones and their potential biomedical applications. Mater Sci Eng C. 2018;91:899–911.
14. Mohandes F, Salavati-Niasari M, Fathi M, Fereshteh Z. Hydroxyapatite nanocrystals: Simple preparation, characterization and formation mechanism. Mater Sci Eng C. 2014;45:29–36.

15. Zhao J, Dong X, Bian M, Zhao J, Zhang Y, Sun Y, et al. Solution combustion method for synthesis of nanostructured hydroxyapatite, fluorapatite and chlorapatite. Appl Surf Sci. 2014;314:1026–33.
16. Kumta PN, Sfeir C, Dong-Hyun L, Olton D, Choi D. Nanostructured calcium phosphates for biomedical applications: novel synthesis and characterization. Acta Biomater. 2005;1(1):65–83.
17. Leventouri TH. Synthetic and biological hydroxyapatites: crystal structure questions. Biomaterials. 2006;27(18):3339–42.
18. Best SM, Porter AE, Thian ES, Huang J. Bioceramics: past, present and for the future. J Eur Ceram Soc. 2008;28(7):1319–27.
19. Kim H-M, Kim Y, Park S-J, Rey C, Lee H, Glimcher MJ, et al. Thin Film of low-crystalline calcium phosphate apatite formed at low temperature. Biomaterials. 2000;21:1129-34.
20. Iafisco M, Ruffini A, Adamiano A, Sprio S, Tampieri A. Biomimetic magnesium–carbonate-apatite nanocrystals endowed with strontium ions as anti-osteoporotic trigger. Mater Sci Eng C. 2014;35:212–9.
21. Chandran S, Shenoy SJ, Babu SS, Nair RP, Varma HK, John A. Strontium Hydroxyapatite scaffolds engineered with stem cells aid osteointegration and osteogenesis in osteoporotic sheep model. Colloids Surf B Biointerfaces. 2018;163:346–54.
22. Venkatesan J, Qian ZJ, Ryu B, Thomas NV, Kim SK. A comparative study of thermal calcination and an alkaline hydrolysis method in the isolation of hydroxyapatite from *Thunnus obesus* bone. Biomed Mater. 2011;6(3):035003.
23. Venkatesan J, Kim SK. Effect of temperature on isolation and characterization of hydroxyapatite from tuna (*Thunnus obesus*) Bone. Materials. 2010;3(10):4761–72.
24. Piccirillo C, Pullar RC, Tobaldi DM, Castro PML, Pintado MME. Hydroxyapatite and chloroapatite derived from sardine by-products. Ceram Int. 2014;40(8):13231–40.
25. Piccirillo C, Adamiano A, Tobaldi DM, Montalti M, Manzi J, Castro PML, et al. Luminescent calcium phosphate bioceramics doped with europium derived from fish industry byproducts. J Am Ceram Soc. 2017;100(8):3402–14.
26. Pon-On W, Suntornsaratoon P, Charoenphandhu N, Thongbunchoo J, Krishnamra N, Tang IM. Hydroxyapatite from fish scale for potential use as bone scaffold or regenerative material. Mater Sci Eng C. 2016;62:183–9.
27. Huang Y-C, Hsiao P-C, Chai H-J. Hydroxyapatite extracted from fish scale: effects on MG63 osteoblast-like cells. Ceram Int. 2011;37(6):1825–31.
28. Sousa MJ, Nascimento Ó. Estatísticas da Agricultura e Pesca da Região Autónoma da Madeira. Direcção Regional de Estatística da Madeira. 2018;76.
29. Coelho A. TOPAS-Academic V5 [Internet]. Brisbane Australia; 2012. Disponível em: http://www.topas-academic.net/.
30. Roche KJ, Stanton KT. Measurement of fluoride substitution in precipitated fluorhydroxyapatite nanoparticles. J Fluor Chem. 2014;161:102–9.
31. Swanson HE, Fuyat RK. Standard X-Ray diffraction powder patterns. Natl Bur Stand. 1953;2:5–6.
32. Calvo C, Gopal R. The crystal structure of whitlockite from the palermo quarry. Am Mineral. 1975;60:120–33.
33. ICDD Powder Diffraction File No. 29–1193. in The International Centre for Diffraction Data. Newtown Square, PA, USA
34. Brunauer S, Emmett PHE, Teller E. Adsorption of gases in multimolecular layers. J Am Chem Soc. 1938;60(2):309–19.
35. Piccirillo C, Silva MF, Pullar RC, Braga da Cruz I, Jorge R, Pintado MME, et al. Extraction and characterisation of apatite- and tricalcium phosphate-based materials from cod fish bones. Mater Sci Eng C. 2013;33(1):103–10.
36. Zhang L, Zhang C, Zhang R, Jiang D, Zhu Q, Wang S. Extraction and characterization of HA/β-TCP biphasic calcium phosphate from marine fish. Mater Lett. 2019;236:680–2.
37. Suchanek W, Yashima M, Kakihana M, Yoshimura M. B-Rhenanite (B-NaCaPO4) as weak interphase for hydroxyapatite ceramics. J Eur Ceram Soc. 1998;18:1923–9.
38. Knabe C, Berger G, Gildenhaar R, Howlett CR, Markovic B, Zreiqat H. The functional expression of human bone-derived cells grown on rapidly resorbable calcium phosphate ceramics. Biomaterials. 2004;25(2):335–44.
39. Eppley BL, Stal S, Hollier L, Kumar M. Compartmentalized bone regeneration of cranial defects with biodegradable barriers—Effects of Calcium Sodium Phosphate Surface Coatings on LactoSorb®. J Craniofacial Surg Clin Notes. 2002;13(5):681–6.
40. Koutsopoulos S. Synthesis and characterization of hydroxyapatite crystals: a review study on the analytical methods. J Biomed Mater Res. 2002;62(4):600–12.
41. Rey C, Shimizu M, Collins B, Glimcher MJ. Resolution-enhanced fourier transform infrared spectroscopy study of the environment of phosphate ion in the early deposits of a solid phase of calcium phosphate in bone and enamel and their evolution with age: 2. Investigations in thev 3 PO4 domain. Calcif Tissue Int. 1991;49(6):383–8.
42. Gómez-Morales J, Iafisco M, Delgado-López JM, Sarda S, Drouet C. Progress on the preparation of nanocrystalline apatites and surface characterization: Overview of fundamental and applied aspects. Prog Cryst Growth Charact Mater. 2013;59(1):1–46.
43. Jalota S, Bhaduri SB, Tas AC. A New Rhenanite (β-NaCaPO4) and hydroxyapatite biphasic biomaterial for skeletal repair. J Bio Mat Res. 2006;80B(2):304-16.
44. Bernache-Assollant D, Ababou A, Champion E, Heughebaert M. Sintering of calcium phosphate hydroxyapatite Ca10(PO4)6(OH)2 I. Calcination and particle growth. J Eur Ceram Soc. 2003;23(2):229–41.
45. Wu J, De Antonio ME, Yang B, Liu C, Jia F, Song S. Efficient removal of Hg2+ in aqueous solution with fishbone charcoal as adsorbent. Environ Sci Pollut Res. 2018;25(8):7709–18.

SUPPORTING INFORMATION

Additional supporting information may be found online in the Supporting Information section.

How to cite this article: Ideia P, Degli Esposti L, Miguel CC, Adamiano A, Iafisco M, Castilho PC. Extraction and characterization of hydroxyapatite-based materials from grey triggerfish skin and black scabbardfish bones. *Int J Appl Ceram Technol*. 2021;18:235–243. https://doi.org/10.1111/ijac.13625